X-ray- and Neutron-diffraction Studies with Quasicrystalline and Amorphous Al-V- and Al-Mn-alloys

S. Seehafer, P. Lamparter, and S. Steeb

Max-Planck-Institut für Metallforschung, Institut für Werkstoffwissenschaft, Stuttgart, BRD

Z. Naturforsch. **45a**, 627–638 (1990); received January 20, 1990

Amorphous and quasicrystalline samples of $Al_{84}Mn_{16}$ and $Al_{84}V_{16}$ were produced by sputtering and melt-spinning, respectively. From X-ray and neutron-diffraction-results the total structure factors were evaluated. For amorphous as well as for quasicrystalline $Al_{84}V_{16}$ the partial $S_{Al\text{-}Al}$- and $S_{Al\text{-}V}$-structure factors were obtained, which yield the corresponding partial pair correlation functions, the atomic distances, and the partial coordination numbers. Also some information concerning the partial Bhatia-Thornton correlation functions could be obtained.

Both the amorphous and the quasicrystalline Al-V-alloys show a linear expansion by a factor of 1.03 compared to the corresponding Al-Mn-alloy. The two amorphous alloys can be designed as isomorphous, whereas the quasicrystalline ones show pronounced deviations in the distance between unequal atoms. The shortest atomic distance in amorphous $Al_{84}V_{16}$ is 2.69 Å, being formed by Al-V-pairs with a coordination number 2. The nearest Al-Al-distance amounts to 2.84 Å with a coordination number 8. The partial density-concentration correlation function clearly deviates from the hard sphere model.

With the quasicrystalline specimens, the isomorphous substitution of Mn- and V-atoms is not perfect. The Al-V-correlation is split up, and this is not observed for the Al-Mn-correlation. Comparison of the amorphous and the corresponding quasicrystalline alloy shows some similarities.

1. Introduction

As discussed in a recent paper [1], quasicrystalline $Al_{86}M_{14}$- and $Al_{84}V_{16}$-alloys can be transformed by electron irradiation into amorphous alloys. During this transition the alloys "avoid" the crystalline state. This can be interpreted as an indication for a special structural relationship between the quasicrystalline and the amorphous phase. In the present work we used the method of isomorphous substitution to determine partial structure factors, partial correlation functions, atomic distances, and partial coordination numbers and to compare the two states in both systems.

2. Theoretical fundamentals

In the present paper we use the Faber Ziman [2] – as well as the Bhatia Thornton [3] – formalism. The experimentally obtained total structure factors S^{FZ} and S^{BT} can be represented in terms of three partial structure factors:

$$S^{FZ} = \omega_{AA}(Q)\, S_{AA}(Q) + \omega_{BB}(Q)\, S_{BB}(Q) + \omega_{AB}(Q)\, S_{AB}(Q) \quad (1)$$

with the weighting factors

$$\omega_{AA}(Q) = \frac{c_A^2 b_A^2}{\langle b\rangle^2}, \quad \omega_{BB}(Q) = \frac{c_B^2 b_B^2}{\langle b\rangle^2},$$

$$\omega_{AB}(Q) = \frac{2 c_A c_B b_A b_B}{\langle b\rangle^2};$$

Q = $(4\pi/\lambda)\sin\Theta$ = modulus of the scattering vector,
2Θ = scattering angle,
λ = wavelength,
$\langle b\rangle = c_A b_A + c_B b_B$,
$\langle b^2\rangle = c_A b_A^2 + c_B b_B^2$,
c_i = atomic fraction of component i,
b_i = scattering length of component i.

$$S^{BT} = \omega_{NN}(Q)\, S_{NN}(Q) + \omega_{CC}(Q)\, S_{CC}(Q) + \omega_{NC}(Q)\, S_{NC}(Q) \quad (2)$$

with the weighting factors

$$\omega_{NN}(Q) = \frac{\langle b\rangle^2}{\langle b^2\rangle}, \quad \omega_{CC}(Q) = \frac{c_1 c_2 (\Delta b)^2}{\langle b^2\rangle},$$

$$\omega_{NC}(Q) = 2\,\frac{\langle b\rangle \Delta b}{\langle b^2\rangle}$$

with $\Delta b = |b_A - b_B|$.

The partial functions S_{AA}, S_{BB}, and S_{AB} describe the contributions of all the AA-, BB-, and AB-pairs to the

Reprint requests to Prof. Dr. S. Steeb, Max-Planck-Institut für Metallforschung, Institut für Werkstoffwissenschaft, Seestraße 92, D-7000 Stuttgart.

0932-0784 / 90 / 0500-0627 $ 01.30/0. – Please order a reprint rather than making your own copy.

total structure factor whereas the partial functions S_{NN}, S_{CC}, and S_{NC} describe the contributions of the topological arrangement, of the chemical arrangement, and the correlation between topological and chemical arrangement to the total structure factor, respectively.

The total structure factor is transformed to the total pair correlation function $G(R)$, which describes the pair correlations in real space, by

$$G(R) = 4\pi\varrho_0 R[g(R)-1] = \frac{2}{\pi}\int_0^\infty Q[S(Q)-1]\sin(QR)\,dQ \qquad (3)$$

with

ϱ_0 = mean atomic number density,
$g(R)$ = pair distribution function = $(\varrho(R)/\varrho_0)$,
$\varrho(R)$ = local atomic number density.

The partial pair correlation functions are obtained from the partial structure factors by relations according to (3).

The apparent total number $Z_{tot}(R_1, R_2)$ of atoms in a shell between R_1 and R_2 follows from

$$Z_{tot}(R_1, R_2) = 4\pi\varrho_0 \int_{R_1}^{R_2} R^2 g(R)\,dR. \qquad (4)$$

Correspondingly, the partial coordination numbers Z_{ij} follow from the partial $c_j g_{ij}(R)$. The relation between the Faber Ziman total and partial coordination numbers is given by

$$Z_{tot} = \frac{c_A b_A^2}{\langle b\rangle^2} Z_{AA} + \frac{c_B b_B^2}{\langle b\rangle^2} Z_{BB} + 2\frac{c_A b_A b_B}{\langle b\rangle^2} Z_{AB}. \qquad (5)$$

The partial coordination numbers finally yield the Warren Cowley chemical short range order parameter α [4, 5],

$$\alpha = \frac{Z_{AA} - Z c_A}{Z \cdot c_B} \qquad (6)$$

with

Z_{AA} = number of A-atoms around an A-atom,
Z = average coordination number.

For total segregation α amounts to $+1$, for statistical distribution of the atoms of both kinds α is zero, and for total compound formation α amounts to $-c_A/c_B$ if $c_A \leq c_B$.

3. Experimental

3.1. *Specimen preparation*

3.1.1. Quasicrystalline material

From the starting materials aluminium ($\leq$99.9%), manganese (99.97%), and vanadium (99.7%) the corresponding alloys were melted by induction melting under argon atmosphere and cast into Al_2O_3 (Al-Mn-alloy)- and MgO (Al-V-alloy)-crucibles. Melt-spinning was also done under argon atmosphere using a forged Cu-Cr-Zr-cylinder for the $Al_{84}Mn_{16}$- and a quartz-cylinder for the $Al_{84}V_{16}$-specimen, respectively. The quasicrystalline meltspun specimens were rather brittle and therefore formed no continuous ribbons but only pieces about 2.5 cm long, 4.5–7 mm wide and 20–40 µm thick. TEM-investigations showed the usual two-phase morphology with quasicrystalline grains being embedded in a second phase which in all cases proved to be fcc-Al.

3.1.2. Amorphous material

Since melt-spinning yielded no amorphous Al-Mn- or Al-V-alloys, RF-sputtering under argon atmosphere was used to produce amorphous $Al_{84}Mn_{16}$- and $Al_{84}V_{16}$-specimens. The substrate temperature was room temperature in the first case and liquid nitrogen temperature in the second. As substrate material we chose mylar foil for the X-ray diffraction specimens and Al-foil for the neutron-diffraction specimens. From the Al-foil the amorphous layer could be exfoliated.

3.2. *X-ray diffraction*

3.2.1. Experimental

The X-ray diffraction experiments according to the angular dispersive technique were performed in transmission mode using a computer-controlled Θ-2Θ-goniometer (D500, Siemens) with Mo-Kα-radiation.

3.2.2. Evaluation procedure

For the densities of the materials investigated we used the values calculated for the case of ideal mixing. For the details of the correction for absorption, polarization and Compton scattering we refer to [6] and [7], e.g. The scattering lengths were taken from [8] and corrected for anomalous dispersion [9]. According to [4] the correction for multiple scattering was dropped.

The structure factor $S(Q)$ was obtained from the intensity by normalization according to [10].

The contribution of the structure factor of Al had to be subtracted from the structure factors of the quasicrystalline samples $Al_{84}Mn_{16}$ and $Al_{84}V_{16}$, respectively. The quantitative evaluation [11] yielded a share of fcc-Al-phase of about 14% in the first and about 20% in the latter case. Thus the compositions of the quasicrystalline phases are $Al_{81}Mn_{19}$ and $Al_{80}V_{20}$, respectively, which will be used in the following.

3.3. *Neutron diffraction*

3.3.1. Experimental

The neutron diffraction experiments were carried out in transmission mode using the D20 multidetector instrument (ILL, Grenoble) with the wavelength 0.88 Å for the amorphous alloys ($0.7\ Å^{-1} \leq Q \leq 13.9\ Å^{-1}$). The quasicrystalline alloys were investigated using 2.4 Å ($Q \leq 5\ A^{-1}$), 0.94 Å ($Q \leq 13\ Å^{-1}$), and 0.88 Å. Typically 2.5 g of the powdered specimens were filled into cylindrical vanadium containers with an outer diameter of 7 mm and a wall thickness of 0.1 mm. Only for the amorphous $Al_{84}V_{16}$-specimen a container with an outer diameter of 4 mm and a wall thickness of 12.7 μm was used.

3.3.2. Evaluation procedure

The background and absorption corrections were done according to [12]. Scattering- and absorption cross sections were taken from [13]. In the case of amorphous $Al_{84}V_{16}$, the run of the corrected intensity curve showed, with increasing Q, a bending down which was much stronger than one could expect from the usual inelastic scattering effect. This could be ascribed to the incoherent scattering contribution of a 2.4% hydrogen contamination of the specimen [11].

The subsequent correction for multiple scattering was done according to [14].

The separation of the scattering contribution of fcc Al from the intensity pattern of the quasicrystalline substances was done in a similar way as described in chapter 3.2.2 [11].

4. Results and discussion

4.1. *Amorphous alloys*

4.1.1. Structure factors

Figure 1 shows the total Faber Ziman structure factors as obtained by using X-rays with amorphous

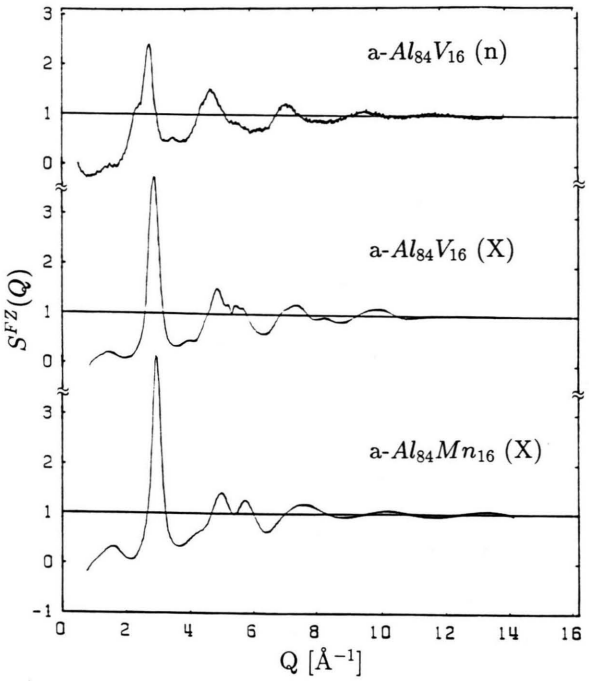

Fig. 1. $S_{tot}(Q)$; *top* curve: amorphous $Al_{84}V_{16}$, neutron diffraction, *middle* curve: amorphous $Al_{84}V_{16}$, X-ray diffraction, *bottom* curve: amorphous $Al_{84}Mn_{16}$, X-ray diffraction.

$Al_{84}V_{16}$ and $Al_{84}Mn_{16}$, respectively and as obtained by using neutrons with amorphous $Al_{84}V_{16}$. The prepeak at $Q \approx 1.6\ Å^{-1}$ indicates a tendency to compound formation in the two alloys [15]. Amorphous $Al_{72}Mn_{22}Si_6$, which was also produced by sputtering, shows a nearly identical run of the structure factor [16]. For the X-ray $Al_{84}V_{16}$-structure factor in Fig. 1 we observe the maxima positions to lie at smaller Q-values, corresponding to larger atomic distances compared to those of $Al_{84}Mn_{16}$. Since the X-ray-scattering lengths of V and Mn are nearly the same, by combination of the X-ray-results in Fig. 1 no further information about partial functions can be expected. This is the case, however, if we combine the X-ray- and the neutron-total structure factors S^X_{tot} and S^N_{tot} for which stands:

$$S^X_{tot} = 0.56\, S_{Al\text{-}Al} + 0.06\, S_{V\text{-}V} + 0.38\, S_{Al\text{-}V}, \quad (7)$$

$$S^N_{tot} = 1.04\, S_{Al\text{-}Al} - 0.04\, S_{Al\text{-}V}. \quad (8)$$

The X-ray weighting factors in the upper equation are given at $Q = 0$.

According to (8), the S^N_{tot}-curve in Fig. 1 (upper curve) can practically be regarded as the partial structure factor $S_{Al\text{-}Al}(Q)$.

The combination of both equations yields the partial Al-V-structure factor $S_{\text{Al-V}}(Q)$:

$$S_{\text{Al-V}} = 2.49\,(S^{\text{X}}_{\text{tot}} - 0.54\,S^{\text{N}}_{\text{tot}} - 0.06\,S_{\text{V-V}}), \qquad (9)$$

Neglecting the $S_{\text{V-V}}$-contribution we thus obtain the run of $S_{\text{Al-V}}$ [11] with an uncertainty of about 12% in the region of smaller Q-values.

4.1.2. Faber Ziman total and partial pair correlation functions

Figure 2 shows the total pair correlation function as obtained by X-ray diffraction with amorphous $Al_{84}Mn_{16}$ in comparison with the corresponding curve of icosahedral $Al_{81}Mn_{19}$.

The same comparison is made in Fig. 3 for the case of amorphous $Al_{84}V_{16}$ and icosahedral $Al_{80}V_{20}$, as well as for the corresponding partial pair correlation functions $G_{\text{Al-Al}}$ and $G_{\text{Al-V}}$.

Table 1 contains the positions of the maxima in the total pair correlation functions and the corresponding coordination numbers as obtained with amorphous $Al_{84}Mn_{16}$ from X-ray diffraction and as obtained with amorphous $Al_{84}V_{16}$ from X-ray diffraction, neutron diffraction, and electron diffraction [1].

The coordination numbers were obtained by the usual Gauß-fitting procedure to the peaks in the $g(R)$-functions.

Looking at the $Al_{84}V_{16}$-data, the main maximum obtained with neutrons lies at the higher R-value of 2.84 Å compared with $R = 2.75$ Å for X-rays. This value corresponds to the Goldschmidt-diameter of Al (2.86 Å) and thus can be identified as Al-Al distance in amorphous $Al_{84}V_{16}$. Note that the neutron result is mainly determined by the Al-Al-contribution (8).

The alloy investigated by electrons was obtained from quasicrystalline material by electron bombardment. The results show that this procedure as well as sputtering is a way of producing amorphous material, the distances being smaller in the latter case by about 3–5%.

Regarding the R-value of the first maximum obtained with electrons and X-rays we state that the larger value obtained with electrons cannot be explained only by the larger electron scattering power of Al; also a structural expansion during the preparation of the electron specimen must have occured. The coincidence between the maximum positions of 2.84 Å as obtained with electron- and neutron-diffraction is supposed to be accidental.

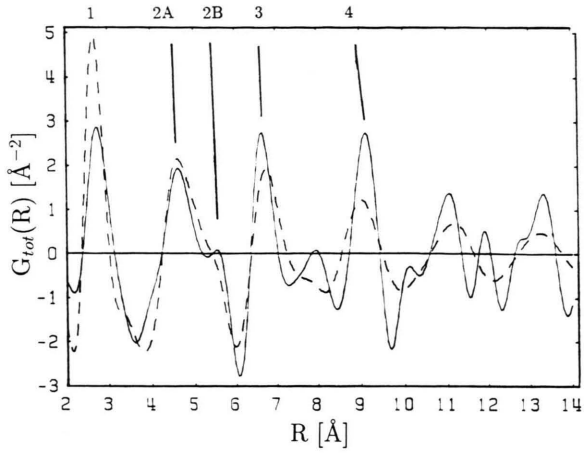

Fig. 2. $G_{\text{tot}}(R)$; X-ray diffraction; (—) icosahedral $Al_{81}Mn_{19}$, (---) amorphous $Al_{84}Mn_{16}$.

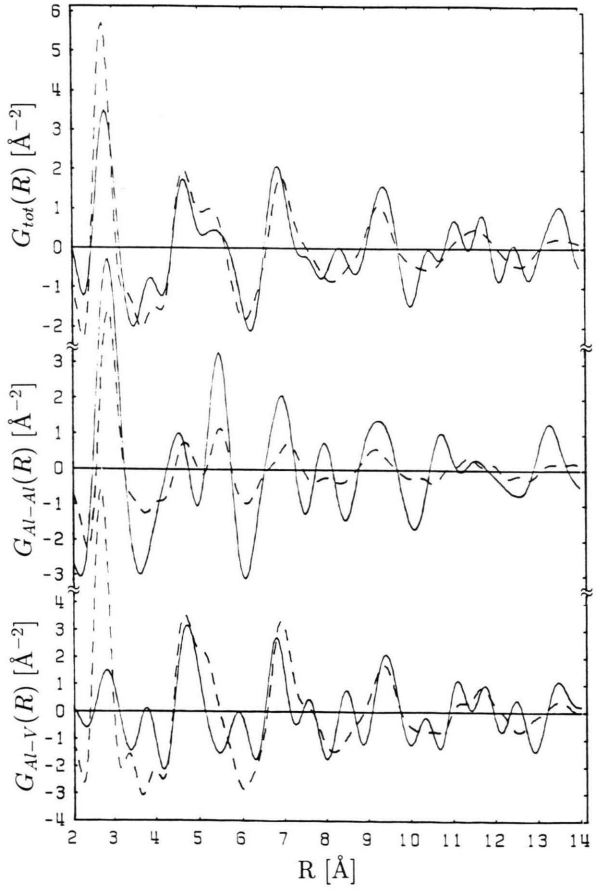

Fig. 3. Icosahedral $Al_{80}V_{20}$ (—) and amorphous $Al_{84}V_{16}$ (---); *top* curve: Total function $G_{\text{tot}}(R)$, X-ray diffraction, *middle* curve: Partial function $G_{\text{Al-Al}}(R)$, neutron diffraction, *bottom* curve: Partial function $G_{\text{Al-V}}(R)$.

Table 1. Distances and coordination numbers of the first four coordination spheres from the $G_{tot}(R)$-curves obtained with amorphous $Al_{84}Mn_{16}$ and amorphous $Al_{84}V_{16}$.

Alloy	Radiation; Function	Number of maximum	R [Å]	Coordination number
$Al_{84}Mn_{16}$	X-rays $G_{tot}(R)$	1	2.68	9.8
		2A	4.64	} 15.8
		2B	≈5.33	
		3	6.82	52.8
		4	9.03	≈116
$Al_{84}V_{16}$	X-rays $G_{tot}(R)$	1	2.75	10.3
		2A	4.66	18.5
		2B	≈5.27	20.9
		3	6.99	84
		4	9.32	≈140
	electrons [1]	1	2.84	~12
		2A	4.86	
		2B	5.54	
		3	7.16	
		4	8.46	
			$R_{Al\text{-}Al}$	$Z_{Al\text{-}Al}$
	neutrons $G_{tot}(R) = G_{Al\text{-}Al}(R)$	1	2.84	7.9
		2A	4.70	12.2
		2B	5.30	21.0
		3	7.14	48.7
		4	9.31	71

Table 2. Amorphous $Al_{84}V_{16}$; $G_{Al\text{-}V}(R)$; peak positions and partial coordination numbers $Z_{Al\text{-}V}$.

Number of maximum	R-value [Å]	Coordination number $Z_{Al\text{-}V}$
1	2.69	1.8
2A	4.61	0.5
2B	5.0	6.1
3A	6.87	1.9
3B	7.25	11.2

As indicated in Table 1, the total pair correlation function obtained with neutrons at the same time stands for $G_{Al\text{-}Al}(R)$. The partial function $G_{Al\text{-}V}(R)$ follows by Fourier-transformation from the partial function $S_{Al\text{-}V}(Q)$ and is presented in Figure 3.

Table 2 contains the Al-V distances and the number of V-atoms around a central Al-atom as obtained from $G_{Al\text{-}V}(R)$.

According to Table 2, 1.8 V-atoms surround each Al-atom at a distance of 2.69 Å. This distance is smaller than the sum of the Al- and V-Goldschmidt-radii which amounts to 2.74 Å. However, the covalent radii, namely 1.47 Å for Al and 1.22 Å for V, exactly yield 2.69 Å.

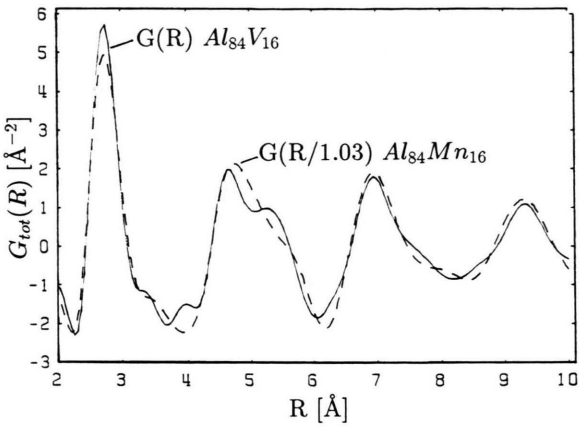

Fig. 4. X-ray diffraction; (—) $G_{tot}(R)$ for amorphous $Al_{84}V_{16}$, (---) $G_{tot}(R)$ for amorphous $Al_{84}Mn_{16}$ rescaled in direction R by a factor of 1.03.

We state that the first sphere around an Al-atom contains 20% V- and 80% Al-contribution.

The second sphere around an Al-atom contains about 83% Al at two distinct distances, namely 12 Al-atoms at 4.70 Å and 21 Al-atoms at 5.3 Å. Furthermore, the second sphere around an Al-atom contains 0.5 V-atoms at the distance 4.61 Å and 6 V-atoms at the distance 5 Å.

Also in the third coordination sphere around an Al-atom we observe a splitting up into three subspheres which contain 2 V-atoms (6.87 Å), 11 V-atoms (7.25 Å), and 49 Al-atoms (7.14 Å), respectively.

Adding the partial coordination numbers $Z_{Al\text{-}Al}$ and $Z_{Al\text{-}V}$ and using the X-ray weighting factors according to (5) yields a total coordination number of 9.54 atoms in the first sphere and of 37.9 atoms in the second sphere. The X-ray measurement yielded 10.3 and 39.4 atoms, respectively.

4.1.3. Comparison between amorphous $Al_{84}V_{16}$ and amorphous $Al_{84}Mn_{16}$

Figure 4 shows the run of $G_{tot}(R)$ in the range $2\text{ Å} \leq R \leq 10\text{ Å}$ for amorphous $Al_{84}V_{16}$ and amorphous $Al_{84}Mn_{16}$. In the plot the latter curve is scaled in R-direction by a factor 1.03. By this procedure both curves become rather congruent. There is only a slight difference in the run of the second maximum where a-$Al_{84}Mn_{16}$ shows only a shoulder instead of a distinct subpeak as observed with a-$Al_{84}V_{16}$. Both spec-

imens therefore are not in a perfect way isomorphous. Apparently the atomic arrangement in Al-Mn is less strictly defined than in Al-V.

4.1.4. Bhatia Thornton partial pair correlation functions

Since amorphous $Al_{84}V_{16}$ contains only 16% V we can assume that direct V-V contacts only exist in a negligible quantity, which means that in the range of the first maximum of $G(R)$ the run of $G_{V\text{-}V}(R)$ can be described by $-4\pi R\varrho_0$. According to [3] the relationships between the Faber Ziman and the Bhatia Thornton partial correlation functions are

$$G_{NN} = c_{Al}^2 G_{Al\text{-}Al} + c_V^2 G_{V\text{-}V} + 2c_{Al}c_V G_{Al\text{-}V}, \quad (10)$$

$$G_{CC} = c_{Al}c_V(G_{Al\text{-}Al} + G_{V\text{-}V} - 2G_{Al\text{-}V}), \quad (11)$$

$$G_{NC} = c_{Al}c_V[c_{Al}(G_{Al\text{-}Al} - G_{Al\text{-}V}) - c_V(G_{V\text{-}V} - G_{Al\text{-}V})]. \quad (12)$$

For amorphous $Al_{84}V_{16}$, Fig. 5 shows the partial Bhatia Thornton correlation functions calculated from $G_{Al\text{-}Al}$ and $G_{Al\text{-}V}$, using $G_{V\text{-}V} = -4\pi R\varrho_0$.

$G_{NN}(R)$ describes the variations of the local atomic number density along R independently of the atomic species. Normally the component with the largest concentration, in this case Al, determines the run of $G_{NN}(R)$.

$G_{CC}(R)$ describes the variations of the concentration along R. For combinations of atoms of unequal species G_{CC} is negative (see (11)). $G_{CC}(R)$ shows a minimum at 2.65 Å, i.e. there are Al-V-correlations at this distance, which agrees well with the Al-V-distance of 2.69 Å as determined from the $G_{Al\text{-}V}$ partial Faber Ziman function.

$G_{NC}(R)$ represents the density-concentration-correlations and depends on the difference of the diameters of the two species. Since the diameters of Al and V are 2.86 Å and 2.26 Å, respectively, G_{NC} as shown in Fig. 5 differs from zero. In the same figure, there is also shown the result of a calculation for a hard sphere model of G_{NC} according to [17]. The much weaker oscillations in the experimental G_{NC} show that the two species do not behave as hard spheres in the amorphous alloy.

4.1.5. Chemical short range order parameter

From the partial coordination numbers in Tables 1 and 2 we obtain, according to (6), the Warren Cowley

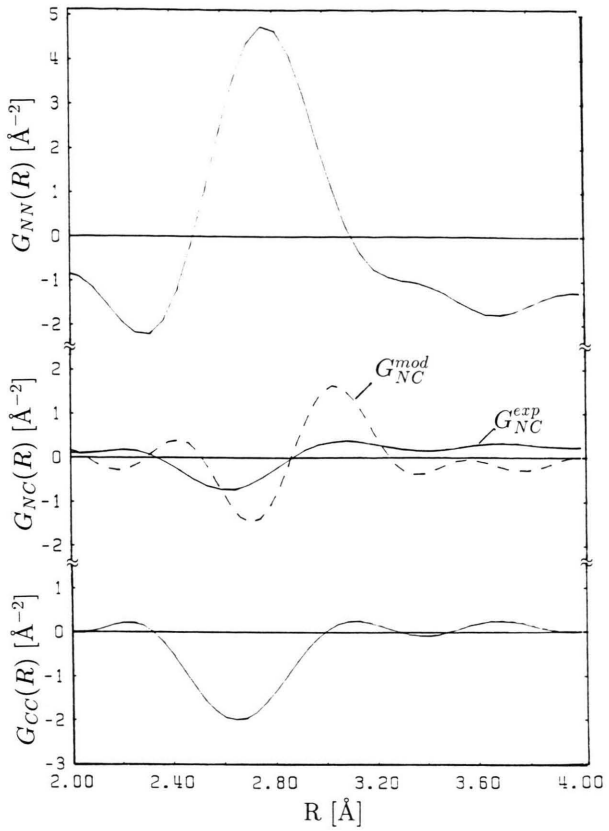

Fig. 5. Amorphous $Al_{84}V_{16}$; Partial Bhatia Thornton correlation functions: *top* curve: $G_{NN}(R)$, *middle* curve: $G_{NC}(R)$ (---) calculated from model, *bottom* curve: $G_{CC}(R)$.

short range order parameter with respect to a central Al-atom for amorphous $Al_{84}V_{16}$:

$$\alpha = \frac{7.9 - 0.84 \cdot 9.7}{0.16 \cdot 9.7} = -0.16. \quad (13)$$

This means a distinct tendency for compound formation (note that $\alpha_{max} = -c_V/c_{Al} = -0.19$).

According to [18] the Warren Cowley chemical short range order parameter also follows from the Bhatia Thornton partial pair correlation functions according to

$$\alpha = \frac{\int_{R_l}^{R_u} RG_{CC}(R)\,dR}{\int_{R_l}^{R_u} (R \cdot G_{NN}(R) + 4\pi R^2\varrho_0)\,dR}. \quad (14)$$

The integration limits R_l and R_u correspond to the limitation of the first coordination sphere in $G_{NN}(R)$, namely $R_l = 2.3$ Å and $R_u = 3.2$ Å. With $\varrho_0 = 0.062$ Å^{-3}

Table 3. Comparison of X-ray- and neutron-diffraction data with icosahedral phases in Al-Mn- and Al-V-alloys. The data for $Al_{86}Mn_{14}$ and $Al_{85}Mn_{14}Si_1$ stem from literature, the data for $Al_{81}Mn_{19}$ and $Al_{80}V_{20}$ are from the present work. I_{rel} are relative intensities. (–) means not observed or no data available.

Indices [19]	X-ray data						Neutron data							
	$Al_{86}Mn_{14}$ [19]		$Al_{81}Mn_{19}$		$Al_{80}V_{20}$		$Al_{86}Mn_{14}$ [20]		$Al_{85}Si_1Mn_{14}$ [21]		$Al_{81}Mn_{19}$		$Al_{80}V_{20}$	
	Q[Å^{-1}]	I_{rel}	Q[Å^{-1}]	I_{rel}	Q[Å^{-1}]	I_{rel}	Q[Å^{-1}]	I_{rel}	Q[Å^{-1}]	I_{rel}	Q[Å^{-1}]	I_{rel}	Q[Å^{-1}]	I_{rel}
(110001) and (32$\bar{1}\bar{1}$2)	1.632	22	1.616	23	1.57	9	1.630	100	1.628	100	1.647	79	1.58	≈7
(1110$\bar{1}$0)	1.876	8	1.86	12	–	–	1.884	56	1.875	77	1.899	89	–	–
(2210$\bar{2}$0)	2.00	–	–	–	–	–	–	–	2.027	1	1.028	20	–	–
(31$\bar{1}\bar{1}$1)	2.20	1.5	–	–	–	–	–	–	2.306	2	2.19	12	–	–
(see text)	–	–	–	–	–	–	2.396	19	–	–	2.401	42	–	–
(21$\bar{1}$001) and (3310$\bar{2}$1)	2.49	3	–	–	–	–	2.486	81	2.49	72	2.486	38	2.41	19
(4410$\bar{4}$1) and (4300$\bar{2}$2)	–	–	–	–	–	–	–	–	2.588	1	2.594	30	–	–
(21$\bar{1}\bar{1}$01)	2.64	–	–	–	–	–	–	–	2.651	17	2.656	100	2.569	36
(2201$\bar{1}$2)	–	–	2.78	9	–	–	–	–	2.853	2	2.776	22	–	–
(100000) and (32$\bar{1}$002)	2.896	100	2.894	55	2.807	85	2.900	50	2.893	26	2.905	30	2.824	80
(110000)	3.043	78	3.032	100	2.945	100	3.038	34	3.038	36	3.031	47	2.958	100
(220002) and (2211$\bar{1}$1)	3.42	1	–	–	–	–	3.286	12	3.243	22	3.296	30	–	–
(111101)	3.44	–	–	–	–	–	3.458	27	3.499	22	3.454	10	3.33	7
(210001)	3.576	1.5	–	–	–	–	3.581	27	3.573	25	3.588	46	3.5	16
(3200$\bar{1}\bar{1}$)	3.63	–	–	–	–	–	–	–	3.63	14	3.68	16	–	–
(2220$\bar{2}$2)	–	–	–	–	–	–	–	–	3.750	3	–	–	3.68	5
(220001)	3.92	0.5	–	–	–	–	3.924	16	3.925	3	3.914	14	3.8	8
(111000) and (3300$\bar{1}$1)	4.200	11	4.2	15	4.07	7	4.209	26	–	–	4.219	20	–	–
(111100)	4.307	3	4.3	8	–	–	4.319	6	–	–	–	–	–	–
(2110$\bar{1}$0)	4.60	0.5	–	–	–	–	4.607	52	–	–	4.679	54	–	–
(320002)	–	–	–	–	–	–	4.765	22	–	–	4.776	57	–	–
(101001)	4.928	20	4.929	44	4.781	35	4.932	27	–	–	4.942	44	4.798	55
(42$\bar{2}$002)	4.99	0.5	–	–	–	–	4.99	5	–	–	–	–	4.932	45
(210000) and (21$\bar{1}$000)	5.32	–	–	–	–	–	–	–	–	–	–	–	≈5.02	25
(2111$\bar{1}$1)	5.51	1	–	–	–	–	–	–	–	–	} 5.58	} 31		
(110010)	5.708	5	5.7	13	5.5	13	–	–	–	–				
(200000) and (111$\bar{1}$00)	5.79	7	5.8	20	–	–	–	–	–	–	–	–	–	–

we obtain $\alpha = -0.2$, which, within the experimental accuracy, is the maximum possible value for $Al_{84}V_{16}$. Thus again, the tendency for compound formation is confirmed for amorphous $Al_{84}V_{16}$.

4.2. *Quasicrystalline alloys*

4.2.1. Intensities and structure factors

The peaks of the icosahedral $Al_{80}V_{20}$- and $Al_{81}Mn_{19}$-alloys as obtained with X-ray and neutron-diffraction are shown in Figs. 6 and 7, respectively. The peak positions and intensities of the present data and some relevant literature data are compiled in Table 3. The X-ray diffraction patterns in Fig. 6 obtained with $Al_{81}Mn_{19}$ and $Al_{80}V_{20}$, respectively, are rather similar, however some peaks in the latter pattern are less pronounced.

The maxima obtained with icosahedral Al-V lie at smaller Q-values (3%) than those of Al-Mn. This is in good correspondence with the amorphous patterns.

The neutron data in Fig. 7 are clearly different from the X-ray data in Figure 6. All peaks in Figs. 6 and 7 besides very few exceptions could be indexed according to the method of Bancel et al. [19]. The quasilattice constant amounts to 4.137 ± 0.007 Å for icosahedral Al-Mn, which is in accordance with literature data. For icosahedral Al-V we obtain 4.259 ± 0.007 Å, i.e. a value which is by 3% larger. Besides the shift in the peak positions the neutron data in Fig. 7 also show strong differences in the peak intensities if we compare

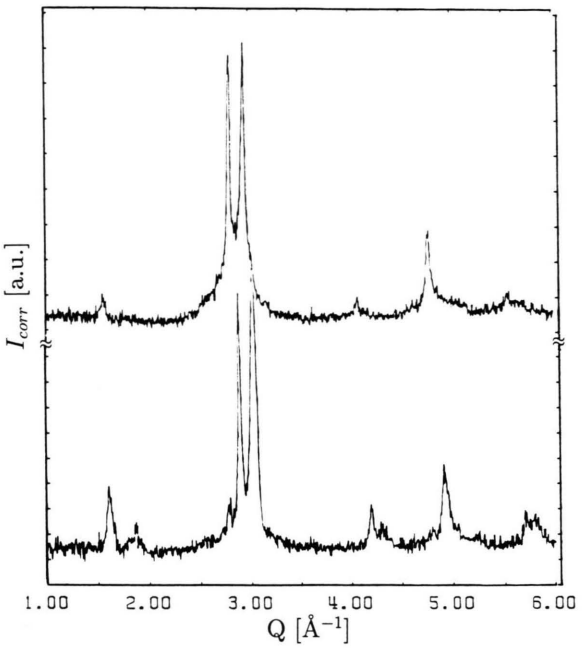

Fig. 6. Peaks of the icosahedral phase; X-ray diffraction; *top* curve: $Al_{80}V_{20}$, *bottom* curve: $Al_{81}Mn_{19}$.

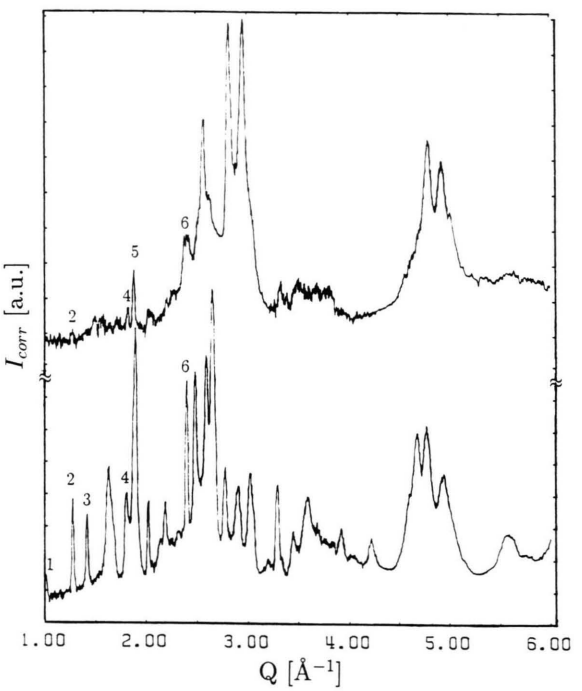

Fig. 7. Peaks of the icosahedral phase; neutron diffraction; *top* curve: $Al_{80}V_{20}$, *bottom* curve: $Al_{81}Mn_{19}$.

Peak No.	Q(Al-Mn) [Å^{-1}]	Q(Al-V) [Å^{-1}]
1	1.01	–
2	1.28	1.27
3	1.42	–
4	1.82	1.82
5	–	1.89
6	2.40	2.40

Table 4. Q-positions of neutron diffraction peaks which do not stem from the icosahedral phase.

the upper with the lower curve. The diffraction pattern of icosahedral $Al_{80}V_{20}$ in Fig. 7 stands for the partial Al-Al structure factor since the weighting factors for the Al-V- and V-V-contributions are very small. Those peaks, marked with numbers in Fig. 7 and listed in Tab. 4, cannot be indexed as icosahedral reflexes.

Peak No. 6 was also found in [20] but could not be indexed in that paper either. The peak positions of Al-V in Table 4 are not shifted by 3%, which we consider as a proof that they are not of icosahedral origin.

Figures 8 and 9 show the total Faber Ziman structure factors as obtained from X-ray- and neutron-diffraction, respectively. The brutto formulas are those which correspond to the real concentrations within the icosahedral phases. The following equations stand for the calculation of partial structure factors:

i-$Al_{81}Mn_{19}$:

$$S_{\text{tot}}^{\text{X}} = 0.48\, S_{\text{Al-Al}} + 0.10\, S_{\text{Mn-Mn}} + 0.42\, S_{\text{Al-Mn}}, \quad (15)$$

i-$Al_{81}Mn_{19}$:

$$S_{\text{tot}}^{\text{N}} = 1.76\, S_{\text{Al-Al}} + 0.11\, S_{\text{Mn-Mn}} - 0.87\, S_{\text{Al-Mn}}, \quad (16)$$

i-$Al_{80}V_{20}$:

$$S_{\text{tot}}^{\text{X}} = 0.48\, S_{\text{Al-Al}} + 0.09\, S_{\text{V-V}} + 0.43\, S_{\text{Al-V}}, \quad (17)$$

i-$Al_{80}V_{20}$:

$$S_{\text{tot}}^{\text{N}} = 1.06\, S_{\text{Al-Al}} \qquad - 0.06\, S_{\text{Al-V}}. \quad (18)$$

The weighting factors given in (15) and (17) for $Q = 0$ are almost identical since the X-ray scattering lengths of Mn and of V are nearly the same. Presuming isomorphous substitution between Mn and V, from (15), (16), and (18) the partial structure factors $S_{\text{Al-Al}}$, $S_{\text{T-T}}$, and $S_{\text{Al-T}}$ (T = V, Mn) could be calculated in principle.

In any case, there is one deviation from ideal isomorphous substitution that has to be considered, namely the shift of the Al-V X-ray curve by 3% with

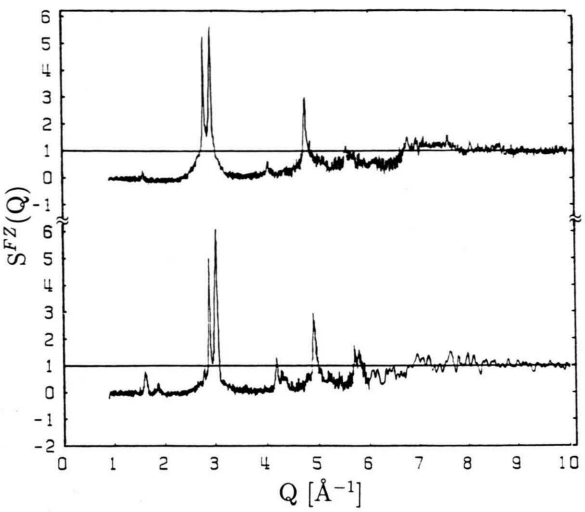

Fig. 8. Total Faber Ziman structure factors; X-ray diffraction; *top* curve: icosahedral $Al_{80}V_{20}$, *bottom* curve: icosahedral $Al_{81}Mn_{19}$.

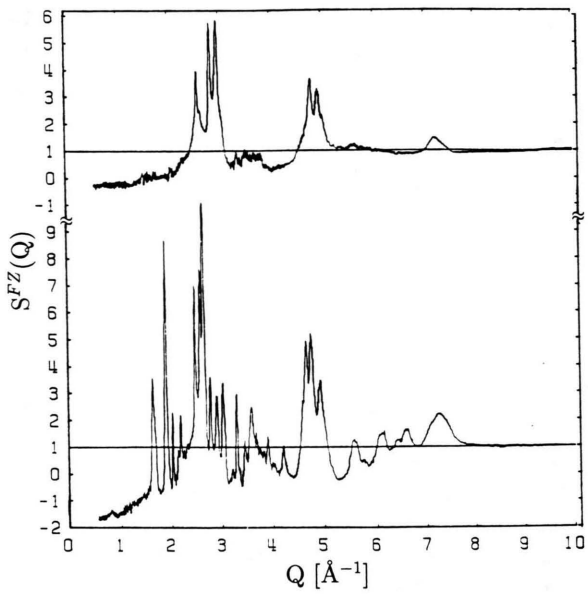

Fig. 9. Total Faber Ziman structure factors; neutron diffraction; *top* curve: icosahedral $Al_{80}V_{20}$, *bottom* curve: icosahedral $Al_{81}Mn_{19}$.

respect to the Al-Mn curve, as already noted above. In calculating the partials this has been taken into account by re-scaling the Q-scale for $S^{N}_{tot}(Al_{80}V_{20})$ by the factor 1.03 before combining (15), (16), and (18). Figure 10, lower curve, shows the resulting partial function $S_{Al\text{-}T}(Q)$.

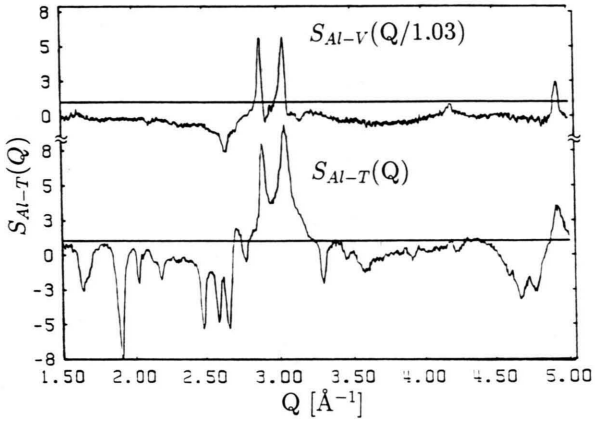

Fig. 10. Comparison of $S_{Al\text{-}V}$ and $S_{Al\text{-}T}$ (see text).

As a crosscheck of the presumption of isomorphous substitution, $S_{Al\text{-}V}(Q)$ was directly calculated from the Al-V data of (17) and (18) without using the Al-Mn data. Hereby, however, $S_{V\text{-}V}(Q)$ had to be neglected, which thus might give rise to an additional error in the order of 10%. Fig. 10, upper curve, shows the resulting $S_{Al\text{-}V}(Q)$, whose Q-scale was multiplied by 1.03 before plotting. In the case of perfect substitution the two curves in Fig. 10 should be the same. We note that all the peaks belonging to $S_{Al\text{-}V}$ also occur in $S_{Al\text{-}T}(Q)$. On the other hand, the $S_{Al\text{-}T}$-curve shows appreciably more peaks with positive and negative amplitudes. From this we have to conclude that the isomorphous substitution between V and Mn is not perfect.

4.2.2. Pair correlation functions

Figure 11 shows the total X-ray pair correlation functions of *i*-$Al_{81}Mn_{19}$ and *i*-$Al_{80}V_{20}$. The corresponding maxima positions and total coordination numbers are compiled in Table 5.

From the partial structure factors $S_{Al\text{-}Al}(Q)$ and $S_{Al\text{-}V}(Q)$, calculated from (17) and (18) as described above, the partial correlation functions $G_{Al\text{-}Al}(R)$ and $G_{Al\text{-}V}(R)$ were obtained and plotted in Figure 12. The $G_{Al\text{-}Al}(R)$ function is practically given by the total neutron $G(R)$ function, as can be seen from (18).

The Al-V distances and coordination numbers are listed in Table 5.

The total X-ray $G(R)$ in Fig. 11 are quite similar, however they differ in some details: In the upper curve, which corresponds to *i*-$Al_{80}V_{20}$, maximum 2A is lower and maximum 2B higher than for *i*-$Al_{81}Mn_{19}$, whereas the total coordination number in the second

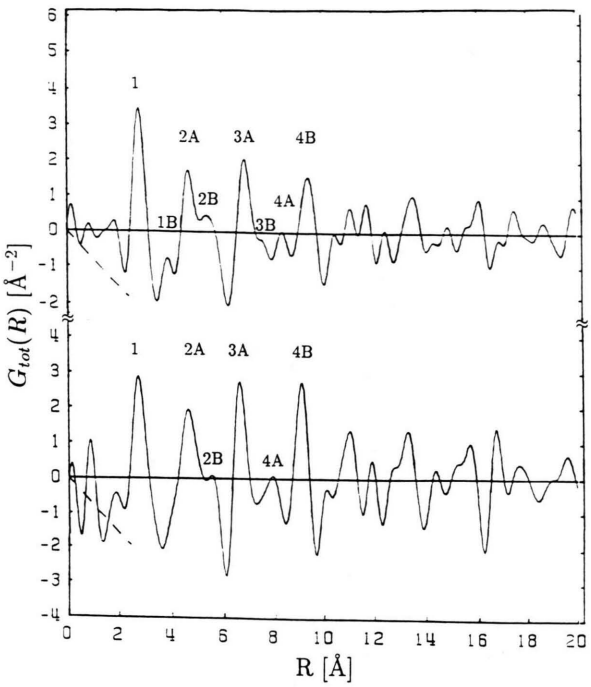

Fig. 11. $G_{tot}(R)$; X-ray diffraction; *top* curve: icosahedral $Al_{80}V_{20}$, *bottom* curve: icosahedral $Al_{81}Mn_{19}$.

Table 5. Distances and coordination numbers of the first four maxima in $G_{tot}(R)$ for *i*-$Al_{81}Mn_{19}$ and in $G_{tot}(R)$ as well as in $G_{Al\text{-}V}$ for *i*-$Al_{80}V_{20}$.

Alloy	Radiation; Function	Number of maximum	R [Å]	Coordination number
i-$Al_{81}Mn_{19}$	X-rays; $G_{tot}(R)$	1	2.75	10.8
		2A	4.63	28.7
		2B	5.58	15.2
		3A	6.65	46.9
		4A	7.96	52
		4B	9.08	83
i-$Al_{80}V_{20}$	X-rays; $G_{tot}(R)$	1	2.80	10.1
		1B	3.88	4.4
		2A	4.66	16.7
		2B	5.38	24.9
		3A	6.86	70
		3B	7.52	70
		4A	8.36	39.6
		4B	9.40	90
			$R_{Al\text{-}Al}$	$Z_{Al\text{-}Al}$
	neutrons; $G_{tot}(R)$ $= G_{Al\text{-}Al}(R)$	1	2.81	10.2
		2A	4.45	12.8
		2B	5.42	23.4
		3A	6.96	43
		3B'	8.03	36
		4B	9.28	83
	−; $G_{Al\text{-}V}$		$R_{Al\text{-}V}$	$Z_{Al\text{-}V}$
		1	2.82	1.5
		1B	3.87	1.2
		2A	4.74	5.4
		2B'	5.89	3.6
		3A	6.82	7.7
		3B	7.57	6.2
		4A	8.48	8.7
		4B	9.43	16.2

sphere is about the same for both phases. With *i*-$Al_{80}V_{20}$ an additional distance 1B is observed, which belongs to the Al-V-correlation, as can be seen by comparison with the partial functions in Figure 12. These differences again show that between *i*-$Al_{80}V_{20}$ and *i*-$Al_{81}Mn_{19}$ no complete isomorphy exists.

From the partial coordination numbers $Z_{Al\text{-}Al}$ and $Z_{Al\text{-}V}$ in Table 5 for the first sphere the short range order parameter $\alpha = +0.36$ follows from (6) for the *i*-$Al_{80}V_{20}$ phase. This is in contrast to the amorphous $Al_{84}V_{16}$-phase, where α is negative, as shown above.

In Table 6 we compare the mean atomic distances and total coordination numbers as obtained from the X-ray $G(R)$ of *i*-$Al_{81}Mn_{19}$ with the partial Al-Al values as obtained in [22] with *i*-$Al_{74}Si_5Mn_{21}$. $G_{Al\text{-}Al}$ obtained with *i*-$Al_{74}Si_5Mn_{21}$ shows a splitting up into two maxima at 4.15 Å and 4.62 Å, whereas in the case of *i*-$Al_{81}Mn_{19}$ only one maximum at 4.63 Å is observed.

Assuming isomorphous behaviour of these two phases we take $Z_{Al\text{-}Mn}$, $Z_{Mn\text{-}Mn}$, and $Z_{Al\text{-}Al}$ from *i*-$Al_{74}Mn_{21}Si_5$ [22] using the weighting factors for *i*-$Al_{81}Mn_{19}$ and then obtain $Z_{tot} = 11.8$ for *i*-$Al_{74}Mn_{21}Si_5$ which agrees fairly well with 10.8 from Table 6.

From this it follows that the structure of the *i*-$Al_{74}Mn_{21}Si_5$-phase investigated in [22] seems to be very similar to the structure of the *i*-$Al_{81}Mn_{19}$-phase.

Within the first coordination sphere in Fig. 12 nearly identical Al-Al- and Al-V-distances occur at 2.81 Å and 2.82 Å. Thus the shortest atomic distance between Al and V at 2.69 Å as observed with amorphous $Al_{84}V_{16}$ does not occur in *i*-$Al_{80}V_{20}$. This means that between Al and V within the icosahedral phase no direct contact occurs as is the case between Al and Mn in *i*-Al_6Mn and *i*-$Al_{74}Mn_{21}Si_5$ according to EXAFS investigations [23, 24] as well as to scattering experiments [22].

For *i*-$Al_{74}Mn_{21}Si_5$ in [22] $Z_{AL\text{-}Mn}$ was reported to be 2.52 atoms. Here we find $Z_{Al\text{-}V} = 1.5$ atoms. If we add the 1.2 atoms belonging to the maximum 1B

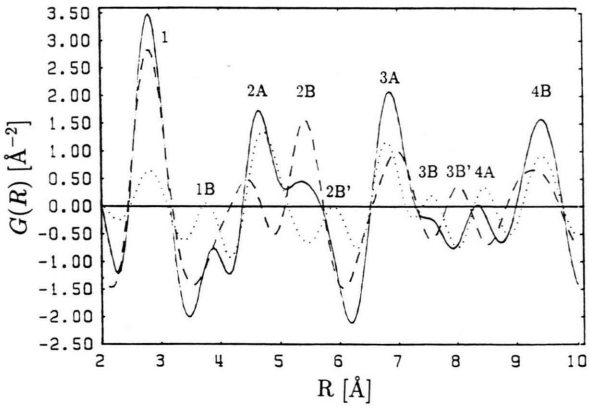

Fig. 12. Icosahedral $Al_{80}V_{20}$; (—) X-ray $G_{tot}(R)$, (----) $\omega_{Al\text{-}Al}G_{Al\text{-}Al}(R)$, (····) $\omega_{Al\text{-}V}G_{Al\text{-}V}(R)$.

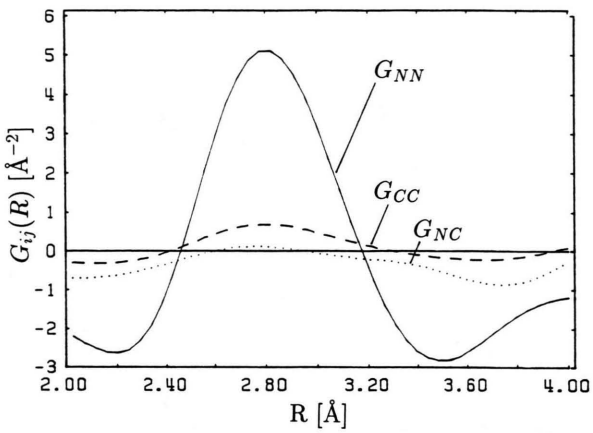

Fig. 13. Icosahedral $Al_{80}V_{20}$; Partial Bhatia Thornton correlation functions.

Table 6. *i*-$Al_{74}Mn_{21}Si_5$ [22]: $R_{Al\text{-}Al}$ and $Z_{Al\text{-}Al}$; *i*-$Al_{81}Mn_{19}$: mean atomic distances and Z_{tot}.

i-$Al_{74}Mn_{21}Si_5$ [22]		*i*-$Al_{81}Mn_{19}$ [present paper]	
$R_{Al\text{-}Al}$ [Å]	$Z_{Al\text{-}Al}$	Mean atomic distances [Å]	Z_{tot}
2.82	9.5	2.75	10.8
4.15 }	16.3	–	–
4.62 }		4.63	28.7
5.45	20.1	5.58	15.2
6.72	6.96	6.65	46.9

at 3.78 Å, the accordance between *i*-Al-Mn(Si) and *i*-$Al_{80}V_{20}$ is rather good.

As in the amorphous alloys also in the icosahedral alloys the distances obtained from the total $G(R)$-functions are larger in the case of the Al-V-alloy than in the case of the Al-Mn-alloy (with exception of distance 2B).

In the *i*-$Al_{80}V_{20}$-alloy we find 47 Al-atoms and 12 V-atoms within a sphere of 6.08 Å radius around an Al-atom, corresponding to a stoichiometry $Al_{80}V_{20}$. The resulting mean atomic number density amounts to 0.0626 $Å^{-3}$, which is in accordance with the value 0.0623 $Å^{-3}$, calculated for the case of ideal mixing.

A comparison of the $G(R)$-functions in Figs. 2 and 3 as obtained with amorphous and icosahedral Al-T-alloys (T = V, Mn) shows rather pronounced similarities. For the Al-Mn-phases this was already concluded from EXAFS-measurements [25]. Of course, as was to be expected, the $G(R)$ curves of the icosahedral phases show more pronounced peaks than those of the amorphous phases.

The most obvious differences in the short range order were observed between $G_{Al\text{-}V}(R)$ of the amorphous and the quasicrystalline $Al_{80}V_{20}$-phase (see Figure 3): The latter shows the pronounced splitting up of the first sphere as already discussed above.

As already done for the amorphous Al-V-phase, in Fig. 13 we also present the Bhatia Thornton correlation functions for the icosahedral $Al_{80}V_{20}$-phase, obtained by using the assumption that the contribution of $\varrho_{V\text{-}V}$ is negligible within the range of the first coordination sphere. The function $G_{NN}(R)$ shows a pronounced peak at 2.8 Å caused by the Al-Al- and the Al-V nearest neighbours in the icosahedral phase. $G_{CC}(R)$ shows a positive first maximum, which indicates that the Al-Al contributions are larger than expected for the case of statistical distribution of Al and V. This corresponds to the positive value of α as calculated above. Since the first Al-Al- as well as the first Al-V-distance lie at the same position, the difference in atomic diameters of the Al- and V-atoms in the icosahedral phase plays no role and therefore $G_{NC}(R)$ is nearly zero. This is a distinct contrast to the amorphous phase.

Acknowledgements

Thanks are due to ILL (Grenoble) for allocation of beam time and to Dr. P. Convert for his useful advices during the measurements.

[1] J. Mayer, K. Urban, J. Härle, and S. Steeb, Z. Naturforsch. **42a,** 113 (1987).
[2] T. E. Faber and J. M. Ziman, Phil. Mag. **11,** 153 (1965).
[3] A. B. Bhatia and D. E. Thornton, Phys. Rev. **B2,** 3004 (1970).
[4] B. Warren, X-Ray-Diffraction, Addison Wesley Verlag 1969.
[5] J. M. Cowley, J. Appl. Phys. **21,** 24 (1950).
[6] K. Sagel, Tabellen zur Röntgenstrukturanalyse, Springer-Verlag, Berlin 1958.
[7] C. N. J. Wagner, J. Non-Cryst. Sol. **31,** 1 (1978).
[8] J. H. Hubbel, W. J. Veigele, E. A. Briggs, R. T. Brovc, D. T. Cromer, and R. J. Howeston, J. Phys. Chem. Ref. Data **4,** 471 (1975).
[9] D. T. Cromer, Acta Cryst. **18,** 17 (1965).
[10] N. S. Gingrich, Rev. Mod. Phys. **15,** 90 (1943).
[11] S. Seehafer, Thesis work, Universität Stuttgart (1989).
[12] H. H. Paalman and C. J. Pings, J. Appl. Phys. **33,** 2635 (1962).
[13] L. Koester and W. B. Yelon, Neutr. Diffr. Newslett. (1983).
[14] J. A. Blech and B. L. Averbach, Phys. Rev. **4A,** 1113 (1965).
[15] S. Steeb, S. Falch, and P. Lamparter, Z. Naturforsch. **75,** 599 (1984).
[16] J. L. Robertson, S. C. Moss, and K. G. Kreider, Phys. Rev. Lett. **60,** 2062 (1988).
[17] N. W. Ashcroft and D. C. Langreth, Phys. Rev. **156,** 685 (1967).
[18] H. Ruppersberg and H. Egger, J. Chem. Phys. **63,** 4095 (1975).
[19] P. A. Bancel, P. A. Heiney, P. W. Stephens, A. I. Goldman, and P. M. Horn, Phys. Rev. Lett. **54,** 2422 (1985).
[20] R. Bellissent, F. Bourrée-Vigneron, and P. Saintfort, J. de Phys. **47,** Coll. **C3,** 361 (1986).
[21] J. Pannetier, J. M. Dubois, C. Janot, and A. Bilde, Phil. Mag. **B55,** 435 (1987).
[22] J. M. Dubois et al., Proceedings of the I.L.L./CODEST Workshop on Quasicrystalline Materials, Grenoble, 1988, World Scientific, 3–18.
[23] P. A. Heiney, P. A. Bancel, A. I. Goldman, and P. W. Stephens, Phys. Rev. B, **34-10,** 6746 (1986).
[24] M. A. Marcus, H. S. Chen, G. P. Espinosa, and C. L. Tsai, Sol. St. Comm. **58-4,** 227 (1986).
[25] J. B. Boyce, F. G. Bridges, and J. J. Hauser, J. de Phys. **47,** Coll. 8 (1986).